RSC Advances

ROYAL SOCIETY OF CHEMISTRY

www.rsc.org/advances

Graphical Abstract:

A novel magnetic alginate-based biosorbent, aiming for efficient removal of Cr(VI) from aqueous system, was successfully synthesized.

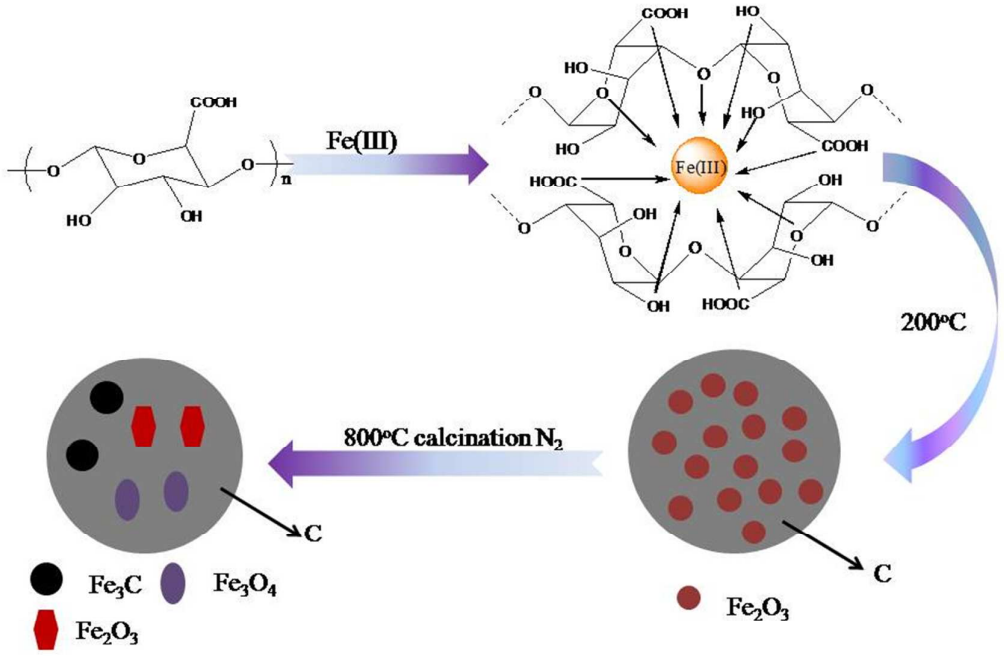

Sodium alginate-based magnetic carbonaceous biosorbents for highly efficient Cr(VI) removal from water

Zhimin Lei, Shangru Zhai*, Jialiang Lv, Yuan Fan, Qingda An*, Zuoyi Xiao

Faculty of Light industry and Chemical Engineering, Dalian Polytechnic University, Dalian 116034

*Corresponding authors.

E-mail: zhaisr@dlpu.edu.cn (S.-R. Zhai); anqingda@dlpu.edu.cn (Q.-D. An)

Abstract

Sodium alginate-derived magnetic carbonaceous materials (Fe-SA-X, X means heating temperature) were fabricated by carbothermal reduction of ferric alginate, aiming for efficient removal of Cr (VI) from water. The materials were characterized by X-ray diffraction patterns, scanning electron microscopy, transmission electron microcopy, Fourier transform infrared spectra, X-ray photoelectron spectroscopy, nitrogen sorption, and Raman spectrometry. The adsorption conditions for Cr (VI) onto the samples were optimized, and adsorption kinetics and isotherm studies were thoroughly studied. The adsorption data fitted well with the pseudo-second-order model and Langmuir isotherm model. The Fe-SA-800 was much more efficient than both Fe-SA-400 and Fe-SA-600, and the maximum adsorption capacity was calculated to be 86.32 mg g^{-1} based on the Langmuir model. The adsorption mechanism was fully discussed, and desorption and regeneration experiments showed that Fe-SA-800 could be easily regenerated and reused. The above results showed that resulting magnetic biosorbents are promising for toxic Cr (VI) removal from water.

Keywords: Cr (VI); Sodium alginate; Biosorbent; Magnetic; Recyclability

1. Introduction

Environmental pollution by chromium has become one of the key environmental health problems facing humanity. Cr(VI) and Cr(III) are two main oxidation states of chromium in aqueous systems, which originate from the wide usage of chromium in electroplating, printing pigments, and other industries .[1] Trivalent chromium are much less toxic than hexavalent chromium, since Cr(VI) possess a serious threat to the ecological environment and human health due to its typical speciation as anionic chromate or dichromate, making it highly mobile in the aqueous media. [2, 3] Chromium is classified by the International Agency for Research on Cancer at the top priority list of pollutants. The maximum authorized in aqueous system is restricted at 5 mg L^{-1}.[4,5] Thus, it is necessary to develop simple and effective methods to remove Cr(VI) from the aqueous system, in order to avoid a hazardous effect on human health.

Recently, numerous treatment technologies have been developed to remove Cr(VI) from aqueous systems. The general methods contained chemical precipitation, [6] adsorption,[4,5] biological treatment and electrochemical treatment.[7] Among all these strategies, adsorption has proved to be the most efficient and widely used one because of its easiness in operation, cost-effectiveness and environmental friendliness as fewer harmful byproducts are formed. Up to now, various adsorbents have been used for the removal of Cr(VI) from aqueous solution including activated carbon,[8] carbon nanotube sheets,[9] graphene oxide,[10] bio-sorbents,[11,24] metal oxides,[12] and hydrogel beads.[13] For instance, Gopalakannan et al. have reported a method to synthesize Fe_3O_4@Alg-Ce magnetic composite beads by incorporating Fe_3O_4 particles onto alginate biopolymer followed by cross-linking with Ce^{3+} ions. The magnetic alginate beads possessed a sorption capacity of 14.29 mg/g.[13] However, because of its poor adsorption capacity and mechanical stability, the Fe_3O_4 particles needed to be

synthesized by extra process; accordingly, its practical application had been restricted to some degree. Contrarily, carbon-based adsorbents are of increasing interest because of their inertness to surrounding environment, mechanical stability and high porous structure with specific surface chemical properties.[14]

Sodium alginate (SA) is one of the natural polymers which possess advantages like high molecular-weight, non-toxic, selective, efficient and inexpensive, which can be cross-linked with different higher valence metal ions, [15, 36] such as Co(III), Fe(III). As we know, The Fe (III) can be transformed into magnetic material followed by carbothermal reduction.[16, 17] The magnetic material makes the rapid and facile separation possible by an external magnetic field.[18,37] More significantly and compared to traditional recovery process, magnetic separation is relatively rapid and easy, cost effective and highly efficient.

Since most of sodium alginate based materials focused on the fabrication of hydrogel beads for the application, scant report on the preparation of sodium alginate based carbonaceous functional materials. Furthermore, to make full use of the function of magnetic character and stability of carbon-based material, and following on continuous interest in designing functional sorbents for emerging pollutants,[6, 19.20.21.22.23, 24] herein a new method to synthesize magnetic carbonaceous materials from Fe^{3+} gelled sodium alginate through facile carbothermal reduction treatment is reported. The economic sodium alginate and $FeCl_3 \cdot 6H_2O$ were chosen as the carbon precursor and magnetic precursor, respectively. The materials were utilized for Cr (VI) adsorption under batch process. The study on the adsorption kinetics and isotherm models was also conducted. As far as the combined characters of low-cost, effective adsorption capacity, facile recovery and recyclability are concerned, it can be considered as a promising biosorbent for Cr (VI) removal from water.

2. Materials and methods

2.1. Chemicals

Sodium alginate and $FeCl_3 \cdot 6H_2O$ were purchased from Sinopharm Chemical Reagent Corporation, China. $K_2Cr_2O_7$, Ethanol, HCl and NaOH were purchased from Tianjin Kermel Chemical Reagent Factory, China. All of the Reagents were of analytical grade and were used as received without any further purification. Double distilled deionized water was used throughout this study. Various Cr(VI) solutions with different concentration were prepared by dissolving $K_2Cr_2O_7$ in deionezed water.

2.2. Preparation of the Fe-SA-X

About 4.0 g of sodium alginate was added to 200 mL distilled water and stirred vigorously for 12 h. Then the above mixture was added dropwise into 5% $FeCl_3$ (w/v) solution for cross-linking to get SA-Fe(III) hydrogel beads and left undisturbed in Fe(III) solution for 6 h for complete cross linking. Finally, the beads were washed with distilled water followed by ethanol and dried in hot air oven at 60 ^oC for 24 h. The dried beads preheated at 200 ^oC for 6 h and then were grinded into powder; the resulted preoxidized carbonaceous material was then heated at a rate of 5 ^oC min^{-1} to a designed temperature (400, 600, or 800^oC) in a N_2 atmosphere and kept for 4 h. After being cooled in flowing N_2, the sample was washed with diluted hydrochloride acid to remove the external Fe and iron oxide. The obtained materials were denoted as Fe-SA-X (X = 400, 600, 800), corresponding to varied heating temperatures.

(Scheme 1.)

2.3 Characterization

X-ray diffraction (XRD) patterns were obtained with a Shimadzu XRD-6100 diffractometer with Cu-K_α radiation (λ = 1.540 Å) from 10 to 80 ^{o} at 8 ^{o} min^{-1}

scanning speed. The surface morphologies and the particle distribution of Fe-SA-X were determined by scanning electron microscopy (SEM, JSM-6460LV, JEOL, Japan) and transmission electron microcopy (TEM, JEM-2000EX electron microscope, JEOL, Japan), respectively. Fourier transform infrared (FTIR, Perkin-Elmer, USA) spectra in the 4000–400 cm^{-1} region were acquired by using KBr pellets. X-ray photoelectron spectroscopy (XPS) measurements were performed using the Thermo Scientific ESCALAB250 spectrometer (Thermo VG, USA) equipped with an Al-Ka X-ray source (1486.6 eV). The specific surface area and pore diameter of the samples were performed by nitrogen adsorption-desorption experiments at 77 K (Quantachrome Autosorb NOVA2200e, USA). Raman spectrometry (RM2000, Renishaw, UK) was used to study the integrity of Fe-SA-X.

2.4 Adsorption experiments and measurements

Batch experiments were conducted in a temperature-controlled shaker. The speed of the shaker was fixed at 300 rpm for all experiments. In order to optimize Cr (VI) removal conditions, the effect of pH, contact time, initial Cr (VI) concentration, temperature and ion strength were investigated. The pH values were adjusted by using 0.1 M HCl or 0.1 M NaOH solution. For batch adsorption experiments, about 20 mg of Fe-SA-X adsorbent were added to the 50 mL conical flask containing 20 mL of Cr (VI) solution with 25 mg/L as the initial concentration. Subsequently, the resulting mixture was stirred to reach equilibrium except kinetic experiments. After equilibration, the suspension were separated by external magnetic field, the supernatant was filtered using 25mm 0.45 um membrane filter, and the filtrate was then analyzed by an UV-Vis spectrophotometer at λ=540 nm with 1, 5-diphenylcarbazide.[25]

The equilibrium adsorption capacity was calculated using the following equation:

$$Q_e = \frac{(C_0 - C_e)V}{M}$$

where, Q_e (mg g^{-1}) is the equilibrium adsorption capacity, C_0 and C_e are the initial and equilibrium concentrations (mg L^{-1}) of Cr(VI), respectively, M (g) is the mass of the dried adsorbent, and V (L) is the volume of the Cr(VI) solutions.

2.5 Adsorption-regeneration for recycling

2 M NaOH solutions were used for the regeneration of the adsorbent. Typically, when the adsorption reaches equilibrium, the adsorbent was separated by external magnetic field and left in the flask. Then, 20 mL, 2 M NaOH solution was added into the conical flask and agitated for 2 h at room temperature followed by washing with distilled water till the pH reach neutral and drying at 60^{o}C in air. The recycling experiment was conducted by using the regenerative adsorbent directly to remove Cr (VI) from freshly prepared Cr(VI) solutions.

3. Results and discussion

3.1 Characterization of Fe-SA-X

The process of fabrication Fe-SA-X materials was depicted in Scheme 1. In the first step, the carboxyl group of SA can form a complex with Fe (III) through the electronic attraction. This process results in binding of numerous iron ions by ion exchange between sodium and ferric ions. Subsequently, the Fe (III) was transformed into Fe_2O_3 through pre-oxidization treatment at 200 ^{o}C for 6 h. Then Fe_2O_3 was transformed into several iron composites by different calcination temperature under an N_2 atmosphere, and the obtained carbonaceous samples can be studied for removal

of Cr(VI) from water. The procedure of pre-oxidization and grinding into powder could decrease the agglomeration of iron species under carbothermal reduction process.

The crystalline structures of the materials carbonized at varied temperatures were characterized by XRD. As seen in Fig. S1, the peaks at 2θ =26.2^{o} in Fe-SA-600 and Fe-SA-800 could be attributed to the diffraction of the (002) plane of the graphite structure,[26] which was due to the carbonization of organic alginate polymer under high temperature, resulting in carbon structures with some degree of graphite order. In Fe-SA-400, the pattern also included Fe_3O_4, Fe_2O_3, [26] according to the reflection peak positions and relative intensities at a carbonization temperature of 400^{o}C. With increasing carbonization temperature, a new peak of Fe_3C was observed, while peaks for Fe_3O_4 and Fe_2O_3 all decreased. When the carbonization temperature reached 800 ^{o}C, peaks were observed for graphite, Fe_3C, and Fe_3O_4. Additionally, it can be noted that the amount of Fe_3C increased significantly, while Fe_3O_4 decreased.[27] Therefore, the carbon-Fe composite materials can be facilely obtained by carbonizing sodium alginate cross-linked with Fe (III) ions.

The scanning electron microscopy (SEM) images of Fe-SA-X samples were shown in Fig. S2. As can be seen, when the calcination temperature reached 400^{o}C, some pores were observed, which was due to the shrinkage of alginate polymer during the carbonization progress. With increasing the temperature, the size of the particles decreased apparently, promoting the development of accessible inter-particle pores.[17] Possibly, for Fe-SA-800, the high porosity would have facilitated the Cr (VI) through the bulk solution to the surface of the adsorbent.[28]

Raman spectroscopy is a powerful tool to characterize the extent of disorder or the degree of carbon crystallinity. The Raman spectra of the Fe-SA-X samples were

displayed in Fig. 1. All samples showed a D peak at 1343 cm^{-1} and 1570 cm^{-1} for G band, respectively, suggestive of the structure of sp^3 and sp^2 hybridized carbon atoms. A low I_D/I_G value indicated the purity of the sample and the high I_D/I_G is the reflective of the higher quality of the carbon-Fe material without defects. The peak intensity ratios (I_D/I_G) were 0.33, 0.49 and 0.71 for Fe-SA-400, Fe-SA-600 and Fe-SA-800, respectively. It was clearly that, with the temperature increasing, the value of I_D/I_G became larger, implying that the carbon atoms of the Fe-SA-800 was more amorphous in nature, leading to more disordered bonds at the atomic level.[9]

(Fig. 1.)

N_2 adsorption-desorption isotherms and pore size distribution curves of the three calcination treatment materials and pre-oxidized materials were depicted in Fig. 2. It reveals that the BET surface areas of the four samples were 18.2, 146.9, 183.5, 203.1 m^2 g^{-1}, respectively. Detailed data were summarized in Table 1. As depicted in Fig. 2A, the specific surface areas increased with increasing carbonization temperature. The increased surface areas may have been caused by decreased the size of the particles, and the expansion of gases such as H_2O and CO_2 formed through the interaction between carbon and iron oxides in the materials at higher temperature treatment under N_2 atmosphere.[26] From the pore size distribution, it was observed that the pore size is less than 5 nm as shown in Fig. 2B. This mesoporous structure was advantageous for mass transfer between the adsorbent and Cr (VI) ions.[30]

(Fig. 2.)

In order to investigate the distribution of magnetic particles in the carbon materials, the TEM results of the three calcination samples were conducted. The images of the samples were depicted in the Fig. S3. As can be seen, the magnetic particles were finely wrapped by the graphene foam which derived from the

carbonization of alginate polymer.[31] The loading of magnetic particles on the foam benefited to increase the surface roughness and render the foam with magnetic property. Additionally, with increasing the carbonization temperature, the particle size decreased gradually, this benefited the development of mesoporous. This phenomenon was consistent with the N_2 adsorption-desorption isotherms.

Furthermore, in order to prove the magnetic property of the Fe-SA-800, the photos of before and after adsorption was depicted in Fig. S4. The sample was dispersed in a certain concentration of Cr (VI) solution, when reached adsorption equilibrium, placing a magnet near to bottle, the black particles were attracted to the wall of the glass bottle quickly and the solution turned transparent within 30 seconds. Therefore, the prepared material can be used as an easily recoverable adsorbent to remove Cr (VI) from aqueous system.

3.2 Cr(VI) adsorption onto magnetic carbonaceous materials

3.2.1 Effect of pH on adsorption

The pH of the Cr (VI) solutions was an important factor which controlled the adsorption process especially on the adsorption performance. This parameter caused the change of surface charge of the sorbent, conversion of the chromium species and other ions present in the solution, and extent of dissociation of functional groups on the active sites of the adsorbent.[32] Accordingly, the adsorption of Cr (VI) ions onto Fe-SA-800 was firstly studied as a function of pH, as depicted in Fig. S5. It was shown that the maximum adsorption capacity was 23.80 mg g^{-1} at pH~ 2; then it continuously dropped to 9.45 mg g^{-1} at pH ~ 10. The Cr (VI) existed in various forms in the aqueous solution, included H_2CrO_4, $HCrO_4^-$, CrO_4^{2-}, and $Cr_2O_7^{2-}$. H_2CrO_4 is predominant when the pH<1.0, $HCrO_4^-$ and $Cr_2O_7^{2-}$ are predominant at pH values ranging from 2.0 to 6.0 and CrO_4^{2-} is predominant at pH>6.0. But the relative

abundance of them are dependent on solution pH and Cr(VI) concentration. Especially, $HCrO_4^-$ could adsorb preferentially on the carbon surface because of its low adsorption free energy.[16] At the pH values ranged from 2.0 to 6.0, the surface of Fe-SA-800 became highly protonated and positively charged, which was benefited to the uptake of Cr (VI) through electrostatic interaction. With increasing the pH value, the carbon surface turned negatively charged, and the electrostatic interaction between the adsorbent and negatively charged Cr (VI) anions became awfully weaken, resulting in the dramatically decreased removal efficiency. Thus, pH 2.0 was selected as a suitable value for the following experiments.

3.2.2 Effect of contact time on Cr (VI) sorption

For optimizing the maximum chromium sorption capacity, sorption experiment were carried out by varying contact time between 5 and 600 min with 25 mg L^{-1} as initial Cr (VI) concentration and 0.02 g as adsorbent dosage at solution pH 2.0. The curves of chromium adsorption by Fe-SA-X were shown in Fig.S6. The adsorption reached equilibrium about 1 h and the adsorption capacity kept constant with further increasing the contact time. By comparing the three samples, the Fe-SA-800 possessed an enhanced sorption capacity of 23.80 mg g^{-1} than both Fe-SA-400 and Fe-SA-600 samples, which possessed capacity of 16.47 and 19.48 mg g^{-1}, respectively.

3.2.3 Effect of initial concentration of Cr (VI) on adsorption

The influence of the initial Cr(VI) concentration on the adsorption capacity of samples were investigated with various concentrations. It can be seen in Fig. S7 that, when the initial concentration increased from 5~500 mg L^{-1}, the sorption capacity of the materials increased from 5 to 85.11 mg g^{-1}. The results showed that the initial Cr (VI) concentration provided a driving force to overcome the mass transfer resistances

between the aqueous system and adsorbent. With more Cr (VI) existed in solution, more active sites of the adsorbent were involved in the adsorption process. Higher ions concentration enhanced the mass transfer driving force, and increased the ions uptake capacity at equilibrium. Additionally, with the increase of Cr (VI) concentrations, the number of collisions between metal ions and adsorbent increased, which enhanced the adsorption process.[32]

3.2.4 Effect of temperature on adsorption

The influence of temperature was investigated by varying temperature at 293, 303 and 313K. As depicted in Fig. S7, with the increase of adsorption temperature, the adsorption capacity increased slightly. At 293K, the capacity increased with the increasing of initial concentration of Cr (VI), and reached maximum adsorption capacity of 85.11 mg g^{-1}. When the adsorption temperature increased to 303K, the capacity increased slightly, as well as the temperature of 313K. The above results showed that the adsorption of Cr (VI) on the Fe-SA-800 surface was not highly dependent on the temperature.

3.3 Adsorption kinetics

In this study, adsorption kinetics was investigated by fitting the experimental data with the pseudo-first-order kinetic model, pseudo-second-order, Elovich equation and intraparticle diffusion kinetic model under the three samples. The rate equation expressed as follows:

$$\log(Q_e - Q_t) = \log Q_e - \frac{k_1}{2.303} t$$

$$\frac{t}{Q_t} = \frac{1}{k_2 Q_e^{\,2}} + \frac{1}{Q_e} t$$

$$Q_t = \frac{1}{b} \ln(ab) + \frac{1}{b} \ln t$$

$$Q_t = K_i t^{1/2} + C$$

where Q_e (mg g^{-1}) and Q_t (mg g^{-1}) are the Cr(VI) amount adsorbed at equilibrium state and at time t (min), respectively; K_1 (min^{-1}), K_2 (g $mg^{-1}min^{-1}$) and K_i (mg $g^{-1}min^{1/2}$) are the rate constants of the pseudo-first-order kinetic model, the pseudo-second-order kinetic model and intraparticle diffusion model, respectively; a (mg $g^{-1}min^{-1}$) is the initial adsorption rate, and b (g mg^{-1}) is related to the extent of surface coverage and the activation energy for the chemisorption; C (mg g^{-1}) is a constant that characterizes boundary layer thickness.

The kinetics parameters obtained were listed in Table 2. It fitted the four kinetic models at the temperature of 293K; the curves were depicted in Fig. 3. It can be observed that the pseudo-second-order model fitted the experimental data better with the correlation coefficients (R^2) values under three samples all above 0.960 and the calculated Q_e was very close to the experimental data. In addition, some literatures[5,18] have also reported that the adsorption of Cr(VI) on the carbon material followed the pseudo-second-order model, which was based on the consumption that chemisorptions is rate-limiting step with the redox reaction and adsorption between the adsorbent and adsorbate.

(Fig. 3.)

3.4 Adsorption isotherms

Adsorption isotherms are important in predictive modeling the procedures for designing the adsorption system, since the adsorption capacity of a quantitative of adsorbent could be described, making the selection of appropriate adsorbent and determination of adsorbent dosage feasible.

In this study, Langmuir isotherm, [33] Freundlich isotherm[34] and Temkin isotherm models were applied to analyze the experimental data. The equations can be expressed as:

$$Q_e = \frac{Q_m K_L C_e}{1 + K_L C_e}$$

$$Q_e = K_F C_e^{1/n}$$

$$Q_e = BLn(AC_e)$$

where Q_e and C_e are the amount of Cr(VI) ions adsorbed (mg g^{-1}) at equilibrium and the equilibrium concentration of Cr(VI) (mg L^{-1}) in the solution; Q_m and K_L are Langmuir constants, which are the adsorption capacity (mg g^{-1}) and energy of adsorption(L mg^{-1}); and K_F and 1/n indicate the adsorption capacity (mg g^{-1}) of the adsorbent and the adsorption intensity. A (L mg^{-1}) and B (mg g^{-1}) are Temkin isotherm constants.

The adsorption constants and correlation coefficients were presented in Table 3, and fitting curves for three temperatures were shown in Fig. 4. The Langmuir isotherm was best described the experimental data, which was apparent from the values of correlation coefficient (R^2) under 293K, 303K, and 313K, that were all higher than the Freundlich model and Temkin model, implying the surface homogeneity of the adsorbent. From the Freundlich model, it was observed that the adsorption intensity (n>1), revealing that the adsorption is favorable.

(Fig. 4.)

Additionally, the essential features of a Langmuir isotherm can be expressed in terms of a dimensionless constant separation factor or equilibrium parameter, R_L which is defined by following equation:

$$R_L = \frac{1}{1 + bCo}$$

where b is the Langmuir constant (L mg^{-1}) and C_o is the initial Cr(VI) ion concentration (mg L^{-1}).

R_L value between 0 and 1 indicates a favorable adsorption. The calculated values of the dimensionless factor R_L were obtained in the range from 0.009 to 0.721, which indicated the favorable adsorption of Cr (VI) over Fe-SA-800. This showed that the equilibrium isotherms can be described by the Langmuir model and the adsorption process was monolayer adsorption onto a surface with finite number of identical sites, which were homogeneously distributed over the adsorbent surface.[32] The comparison with other similar alginate-based and carbon materials were listed in Table 4.

3.5 The effect of coexisting anions strength

As we know, Cr(VI) exist in the form of anions in aqueous phase, and adsorption of Cr(VI) occurs on the adsorbent surface through electrostatic interaction. Thus, the adsorption of Cr(VI) would not been influenced by the cations exist in the solution. Therfore, experiments were performed to study the effect of commonly present anions such as Cl^-, NO^{3-}, SO_4^{2-}, and PO_4^{3-} (C_0 = 200, 400, 800, 2000 mg L^{-1}) on the Cr(VI) uptake. As shown in Fig. S8, all the four anions have the influence of different levels, which is reflected by the following sequence of the Cr(VI) adsorption capacity: Cl^- >NO_3^->SO_4^{2-}>PO_4^{3-}. The Cl^- and NO_3^- had less effect on the removal of Cr(VI), with increasing the concentration of Cl^- and NO_3^-, the adsorption capacity decreased slightly. When the concentration of SO_4^{2-} and PO_4^{3-} increased from 200 to 2000 mg L^{-1}, the adsorption capacity decreased dramatically, and the effect of PO_4^{3-} was much larger than SO_4^{2-}. What can explain this phenomenon is the competition mechanism.[44] As for Cl^- and NO^{3-} are monovalent anions, and they may slightly compete with the

chromium anion for the positive charge adsorption sites on the Fe-SA-800 surface. However, the SO_4^{2-} and the PO_4^{3-} are multivalent anions, which could compete with $Cr_2O_7^{2-}$, $HCrO_4^-$, and CrO_4^{2-} for more available sorption sites of the Fe-SA-800. The study of coexisting anions strength on Cr(VI) uptake demonstrated that electrostatic force is one of possible adsorption mechanism for the removal of Cr(VI).

3.6 Desorption and reusability study

To make the sorption media cost effectively for Cr (VI) removal from the aqueous system, it is important that the samples should be reused for repeated cycles. For repeated use of an adsorbent, adsorbed metal ions should be easily desorbed under suitable conditions. Desorption of the adsorbed Cr (VI) ions from the sample were studied in a batch experimental system and it was depicted in Fig. S9. Desorption experiments put into evidence that after 2 h contact with 20 ml, 2 M NaOH solutions. The recycling test of NaOH solution treated Fe-SA-800 showed that adsorption-desorption process was reversible. Three cycles of adsorption-desorption experiments were conducted to examine the capacity of the sample to retain Cr (VI) ions removal capacity. The adsorption capacity of the material was decreased less than 10% during a three adsorption-desorption cycle. The decline of the performance may be ascribed to the fact that the reduction property of the material to Cr (VI) was diminished after first adsorption. In the subsequent cycles, the adsorption capacity kept constant basically. Desorption and recyclability studies indicated that Fe-SA-800 could be repeatedly used as efficient adsorbent in the process of adsorbing Cr (VI).

3.7 Removal mechanism of Cr (VI) over Fe-SA-X

Many process such as the electrostatic attraction, redox reactions, and precipitation could get involved in the Cr (VI) removal. Within this context, both surface sensitive FTIR and XPS were employed to analyze the adsorption mechanism.

FT-IR spectra of Fe-SA-400, Fe-SA-600, and Fe-SA-800, and after adsorption of Cr (VI) by Fe-SA-800 were depicted in Fig. S10. Before adsorption, the spectra of Fe-SA-X showed analogous peaks, the two bands at around 3440 and 1626 cm^{-1} can be assigned to O-H and C-O stretching vibrations, respectively, which indicated the presence of numerous hydroxyl groups. The band at 1629 and 1384 cm^{-1} corresponding to C=C stretching vibration and C-H symmetric deformation vibration. With increasing the temperature, the intensity of C-H decreased gradually, whereas the O-H remained unchanged. For the four samples, the common bands at 561 cm^{-1} can be due to Fe-O. As illustrated in Fig. S10d, after adsorption of Cr (VI), the intensity of the spectra became weaker than the unabsorbed sample, which was shown in Fig. S10c. It was obviously that the –OH became weaker after Cr(VI) adsorption, and the shift from 3441 to 3434 cm^{-1}, maybe some interaction strengthened between the adsorbent and the Cr (VI) ions, e.g. electrostatic attraction or redox reactions. [16] Through comparing the spectra of before and after adsorption, it notes that a new band at 571.5 cm^{-1}, which can be ascribed to the Cr-O, was clearly observable; this indicated that Cr(VI) species had been enriched onto the sample.[29] Additionally, the shift of C-H from 1110 to 1067cm^{-1} showed that the C-H also participate in the process of removal Cr(VI). [16] The solution pH could make a difference on the reduction ability of C-H bonds of the samples, and when the system was weak acidic, the reduction ability of C-H groups would be strengthened. Therefore, it was possible that it also participated in the adsorption process, which reduced Cr(VI) to Cr (III), and itself was oxidized. No COOH groups that could decompose easily under high temperature was observed to exist on the Cr(VI)-adsorbed Fe-SA-800. The redox reaction and the generation and decomposition of COOH groups may be explained by the following equations:[16]

$$-C-H + Cr(VI)+H_2O \rightarrow -C-OH + Cr(III)+ H^+$$

$$-C-OH + Cr(VI)+H_2O \rightarrow -C=O + Cr(III)+H^+$$

$$-C=O + Cr(VI)+H_2O \rightarrow -COOH + Cr(III) + H^+$$

$$-C-COOH + Cr(VI)+H_2O \rightarrow -C-H + Cr(III) + H^+ + CO_2\uparrow$$

,which was consistent with the following XPS analysis results. Therefore the surface structure of Fe-SA-800 could be remained during the removal process and the amount of reducing groups on the material did not decrease after regeneration, which benefited to its reuse.

To further investigate the mechanism of adsorption, XPS was used to detect the slight change of surface chemistry. As illustrated in Fig. 5a, the photoelectron lines at binding energy of about 574, 708.4, 528.2, 282.4eV were attributed to Cr2p, Fe2p, O1s, and C1s, respectively. By comparing the curves before and after adsorption, two Cr 2p line peaks that locate at 576 and 586eV can be clearly observed. The high resolution chromium region was shown in Fig. 5b, after interaction with Cr (VI), it can be seen that the $Cr2p_{1/2}$ and $Cr2p_{3/2}$ located at 576.5 and 586.5eV, respectively. Each of them could be further fitted into two peaks, the ones at 587.6 and 586.4eV were assigned to the $Cr2p_{1/2}$ of Cr(VI) and Cr(III), while those at 577.4 and 576.2eV to the $Cr2p_{3/2}$ of Cr(VI) and Cr(III), indicating that Cr(VI) and Cr(III) species coexisted on the surface of the sample. Figure 5c and d displayed the C1s spectra of Fe-SA-800 before and after Cr(VI) adsorption, the peaks at 284, 284.7 and 285.3eV ascribed to the C=C, C-H and C-OH, respectively. Comparing with before and after adsorption, no new peak appears, which can be explained by the above redox reaction equations, only the intensity of C-H and C-OH has changed to a certain extent. To our knowledge, C-H and C-OH groups were the strongest reducing groups on the carbon surface.[16] After adsorption onto the surface, possibly, the C-H and –C-OH function

groups could have reduced the Cr (VI) to Cr (III); meanwhile itself was oxidized to C-OH and –COOH, respectively. Afterward, the –COOH transformed into –C-H or –C-OH for its easy decomposition. Finally, the formed Cr(III) was deposited on the carbon surface.

(Fig. 5.)

Based on the above analysis, the whole process of Cr (VI) adsorption should be consisted of the following steps. Firstly, the external mass transfers of Cr (VI) ions occurred from the bulk solution to the adsorbent surface through the electrostatic attraction between the protonated oxygen-contained function groups and the negative $HCrO_4^-$. Then, the Cr (VI) ions diffused into the internal pores of the adsorbent and partial of them were reduced by the C-H or C-OH groups. Finally, Cr(VI) and formed Cr (III) were deposited onto the carbon surface.[29] The possible adsorption mechanism was depicted in Scheme 2.

(Scheme 2.)

4. Conclusion

Low-cost biosorbents for the efficient removal of Cr (VI) from water have been prepared through a facile carbothermal reduction of ferric alginate. It was found that the pseudo-second-order model was able to better describe the adsorption kinetics by comparing the correlation coefficient (R^2). The adsorption isotherm was fitted with the Langmuir model by comparing the correlation value, and the maximum adsorption capacity could reach *ca.* 86.32mg g^{-1}. This kind of biosorbent could be easily regenerated and reused for several consecutive cycles, and the adsorption mechanism was also carefully discussed.

Acknowledgments Financial support from the National Natural Science Foundation of China (21446001), the Program for Liaoning Innovative Research Team in

University (LT2013012) and the Program for Liaoning Excellent Talents in University (LJQ2014056) is highly appreciated.

Supporting Information

Supporting Information include XRD, SEM, TEM, FTIR, VSM curves and the effect of pH, contact time, temperature, initial concentration, ion strength and the reusability test.

Notes and References

1. H. Gu, S.B. Rapole, Y. Huang, D. Cao, Z. Luo, S. Wei, Z. Guo, *J. Mater. Chem. A.* , 2013, **1**, 2011−2021.
2. C.J. Lin, S.L. Wang, P.M. Huang, Y.M. Tzou, J.C. Liu, C.C. Chen, J.H. Chen, C. Lin, *Water Res.*, 2009, **43**, 5015−5022.
3. J. Zhu, S. Wei, H. Gu, S.B. Rapole, Q. Wang, Z. Luo, N. Haldolaarachchige, D.P. Young, Z. Guo, *Environ. Sci. Technol.*, 2011, **46**, 977−985.
4. M. Kebir, M. Chabani, N. Nasrallah, A. Bensmaili, M. Trari, *Desalination*, 2011, **270**, 166-173.
5. A. Kara, E. Demirbel, N. Tekin, B. Osman, N. Besiril, *J. Hazard. Mater.* , 2015, **286**, 612-623.
6. A. Qian, P. Liao, S. Yuan, M. Luo, *Water Res.*, 2014, 48, 326−334.
7. L. Lin, S.R. Zhai, Z.Y. Xiao, Y. Song, Q.D. An, and X.W. Song, *Bioresour. Technol*., 2013,**136**, 437-443.
8. Y. Chen, S.R. Zhai, N. Liu, Y. Song, Q.D. An, and X.W. Song, *Bioresour. Technol*., 2013,**144**, 401-409.
9. V.K. Gupta, S. Agarwal, T.A. Saleh, *Water Res.,* 2011, **45**, 2207–2212.
10. Z.J. Jiang, Y.G. Liu, G.M. Zeng, W.H. Xu, B.H. Zheng, X.F. Tan, S.F. Wang, *RSC Adv*., 2015, **5(32)**, 25389-25397.

11. A. S. K. Kumar, S. J. Jiang, W. L. Tseng, *J. Mater. Chem. A*., 2015, **3**, 7044-7057.

12. S.B. Wu, K.S. Zhang, X.L. Wang, Y. Jia, B. Sun, T. Luo, F.L. Meng, Z. Jin, D.Y. Lin, W. Shen, L.T. Kong, J.H. Liu, *Chem. Eng. J.* ,2015, **262**, 1292-1302.

13. D. Setyono, S. Valiyaveettil, *ACS Sustainable Chem. Eng.*, 2014, **2(12)**, 2722-2729.

14. X.Q. Zhang, Y. Guo, W.C. Li, *RSC Adv.*, 2015, **5(33)**, 25896-25903.

15. V. Gopalakannan, N. Viswanathan, *Int. J. Biol. Macromol.*, 2014, **72**, 862-867.

16. S.X. Chen, H.M. Zeng, *Carbon*, 2003, **41**, 1265–1271.

17. X.L. Li, Y.X. Qi, Y.F. Li, Y. Zhang, X.H. He, Y.H. Wang, *Bioresour. Technol.*, 2013, **142**, 611-619.

18. L.Z. Zhuang, Q.H. Li, J.S. Chen, B.B. Ma, S.X. Chen, *Chem. Eng. J.*, 2014, **253**, 24-33.

19. Y. Li, S.M. Zhu, Q.L. Liu, Z.X. Chen, J.J., Gu, C.L. Zhu, T. Lu, D. Zhang, J. Ma, *Water Res.*, 2013, **47(12)**, 4188-4197.

20. Y. Yi, C.L. Lai, Y.Q. Jiang, J.F. Mei, H. Wang, G.Q. Ying, *J. Appl. Polym. Sci*., 2012, **125**, 248−254.

21. Y. Zhao, S.R. Zhai, B. Zhai, and Q.D. An, *J. Sol-Gel Sci. Technol.*, 2012, **62**, 177-185.

22. J.M. Zhang, S.R. Zhai, S. Li, Z.Y. Xiao, Y. Song, Q.D. An, and G. Tian, *Chem. Eng. J.*, 2013, 215-216, 461-471.

23. S.X. Huang, Z.Y. Xiao, S.R. Zhai, B. Zhai, F. Zhang, Q.D. An, *RSC Adv*., 2014, **4(105)**, 60460-60466.

24. W.J. Qiao, S.R. Zhai, F. Zhang, Z.Y. Xiao, Q.D. An, X.W. Song, *J. Sol-Gel Sci. Technol.*, 2014, **70**, 451-463.

25. P. Guo, S.R. Zhai, Z.Y. Xiao, Q.D. An, *J. Colloid Interface Sci.*, 2015, **446**, 155-

162.

26. H. Guo**,** S.F. Zhang**,** Z.N. Kou**,** S.R. Zhai**,** W. Ma**,** Y. Yang**,** *Carbohyd. Polym*. **,** 2015, **115**, 177-185.

27. B. Qiu, J. Guo, X. Zhang, D.Z. Sun, H.B. Gu, Q. Wang, H.W. Wang, X.F. Wang, X. Zhang, Brandon L. Weeks, Z.H. Guo, S.Y. Wei, *ACS Appl. Mater. Inter*., 2014, **6**, 19816-19824.

28. J.J. Ma, L.C. Zhou, W.F. Dan, H. Zhang, Y.M. Shao, C. Bao, L.Y. Jing, *J. Colloid Interface Sci.*, 2015, **446**,298-306.

29. X. Zhang, Y.X. Li, G.Y. Li, C.W. Hu, *RSC Adv.*, 2015, **5(7)**, 4984-4992.

30. D. H. K. Reddy, S. M. Lee, *Colloid Surf. A-Physicochem. Eng. Asp.*, 2014, **454**, 96-103.

31. C.Y. Cao, J. Qu, W.S. Yan, J.F. Zhu, Z.Y. Wu, W.G. Song, *Langmuir*., 2012, **28**, 4573-4579.

32. G.D. Yang, L. Tang, Y. Cai, G.M. Zeng, P.C. Guo , G.Q. Chen, Y.Y. Zhou , J. Tang, J. Chen, W.P. Xiong, *RSC Adv*. ,2014, **4(102)**, 58362-58371.

31. S. Yang, L. Chen, L. Mu, P.C. Ma, *J. Colloid Interface Sci*. ,2014, **430**, 337-344.

32. M.M Zhang, Y.G. Liu, F.Y. Guo and S.F. Wang, *RSC Adv.***,** 2015, **5**,46955-46964.

33. Langmuir I., *J. Am. Chem. Soc.*, 1918, 40, 1361e8.

34. Freundlich H., *Z. Phys. Chem.*, 1906, **57**, 385-470.

35. H. Chen, X.X. Wang, J.X. Li, X.K. Wang, *J. Mater. Chem. A*, 2015, **3 (11)**, 6073-6081.

36. D.H. Li, D.J. Yang, X.Y. Zhu, D.W. Jing, Y.Z. Xia, Q. Ji, R.S. Cai, H.L. Li and Y.K. Che , *J. Mater. Chem. A*, 2014, **2**, 18761-18766

37. M. S. Moorthy, D.J. Seo, H.J. Song, S. S. Park and C.S. Ha, *J. Mater. Chem. A*, 2013, **1**, 12485-12496

38. J. Zhang, T. Shang, X. Jin, J. Gao and Q. Zhao, *RSC Adv.*, 2015, **5**, 784–790.

39. Z. Ruan, J. Wu, J. Huang, Z. Lin, Y. Li, Y. Liu, Pi. Cao, Y. Fang, J. Xie and G. Jiang, *J. Mater. Chem. A*., 2015, **3**, 4595–4603.

40. M. Zhang, Y. Liu, T. Li, W. Xu, B. Zheng, X.i Tan, H. Wang, Y. Guo, F. Guo and S. Wang, *RSC Adv.*, 2015, **5**, 46955–46964.

41. A. S. K. Kumar, S. Jiang and W. Tseng, *J. Mater. Chem. A*, 2015, **3**, 7044–7057.

42. Y. Li, S. Zhu , Q. Liu , Z. Chen , J. Gu ,C. Zhu , T. Lu , D. Zhang , J. Ma, *Water Res.*, 2013, **47**, 4188-4197.

43. C. Wu, J. Fan, J. Jiang and J. Wang, *RSC Adv.*, 2015, **5**, 47165–47173.

44. G. Yang, L. Tang, Y. Cai, G. Zeng, P. Guo, G. Chen, Y. Zhou, J. Tang, J. Chen and W. Xiong, *RSC Adv.*, 2014, **4**, 58362–58371.

Figure captions:

Scheme 1. Fabrication process of magnetic carbonaceous biosorbents utilizing Fe^{3+} gelled sodium alginate as starting material.

Scheme 2. The mechanism for the removal of Cr(VI) by Fe-SA-X.

Fig. 1. Raman spectra of (a) Fe-SA-400, (b) Fe-SA-600, (c) Fe-SA-800.

Fig. 2. A :The BET of (a) Fe-SA-200, (b) Fe-SA-400, (c) Fe-SA-600, and (d) Fe-SA-800 ; B :The pore diameter diffraction of (a) Fe-SA-200, (b) Fe-SA-400, (c) Fe-SA-600, and (d) Fe-SA-800.

Fig. 3. The (a) pseudo-first-order, (b) pseudo-second-order, (c) Elovich equation and (d) intraparticle diffusion kinetics model of Cr(VI) adsorption on the Fe-SA-X (X represents 400, 600, 800).

Fig. 4. Langmuir, Freundlich and Temkin isotherm model of Cr(VI) adsorption on Fe-SA-800.

Fig. 5. XPS spectra of (a) the survey before and after adsorption, (b) the Cr2p peaks, the C1s pattern of (c) before and (d) after adsorption.

Table 1. The BET parameters of the Fe-SA-X.

Table 2. Kinetic parameters of Cr(VI) adsorption on the Fe-SA-X.

Table 3. Isotherm parameters of Cr(VI) adsorption on Fe-SA-800.

Table4. The Cr(VI) adsorption capacity of Fe-SA-800 compared with other similar materials.

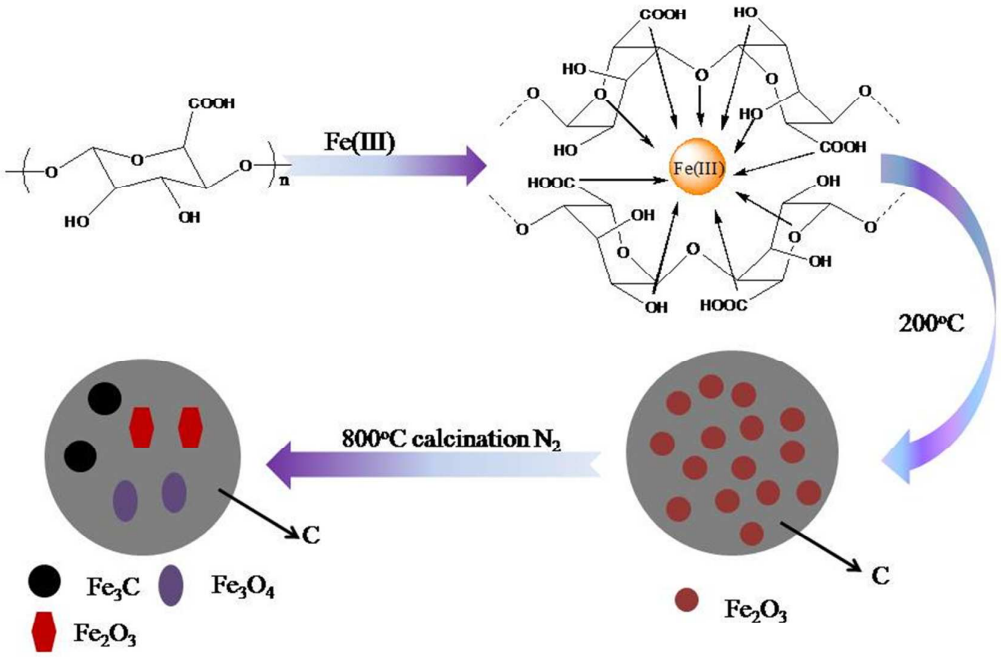

(Scheme 1.)

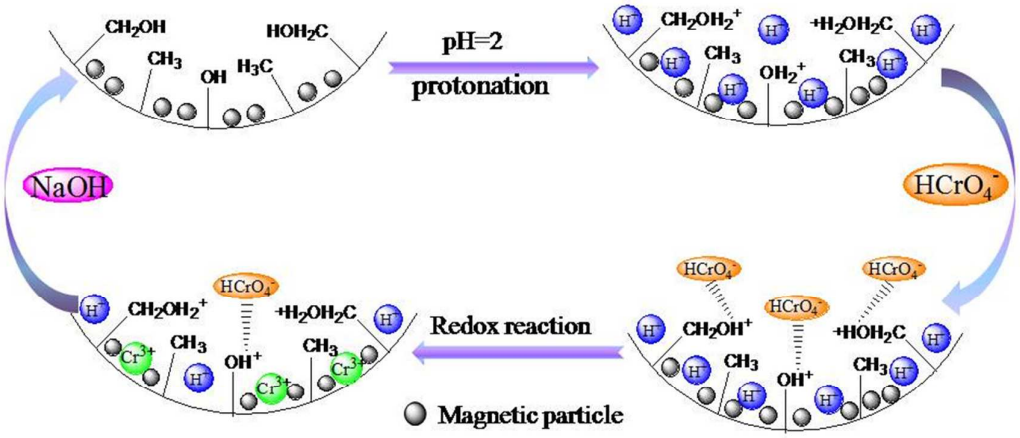

(Scheme 2.)

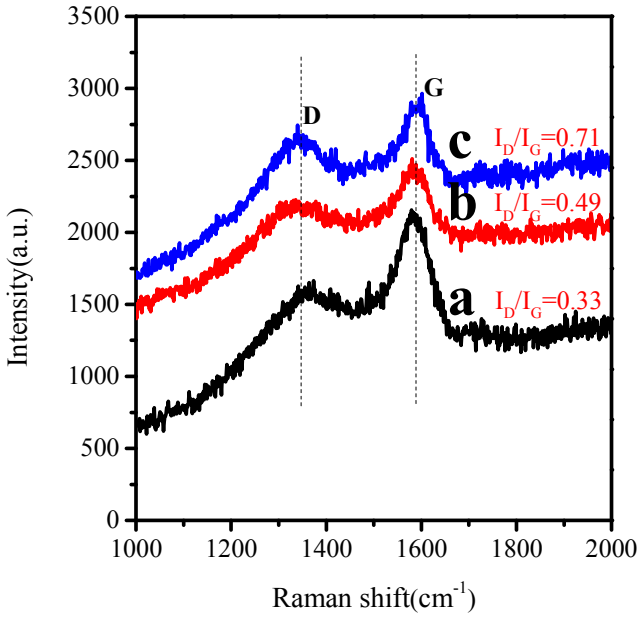

(Fig. 1.)

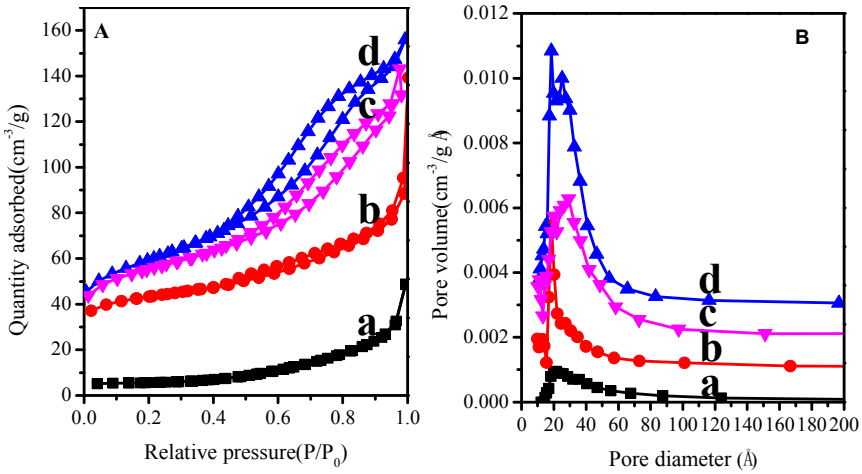

(Fig. 2.)

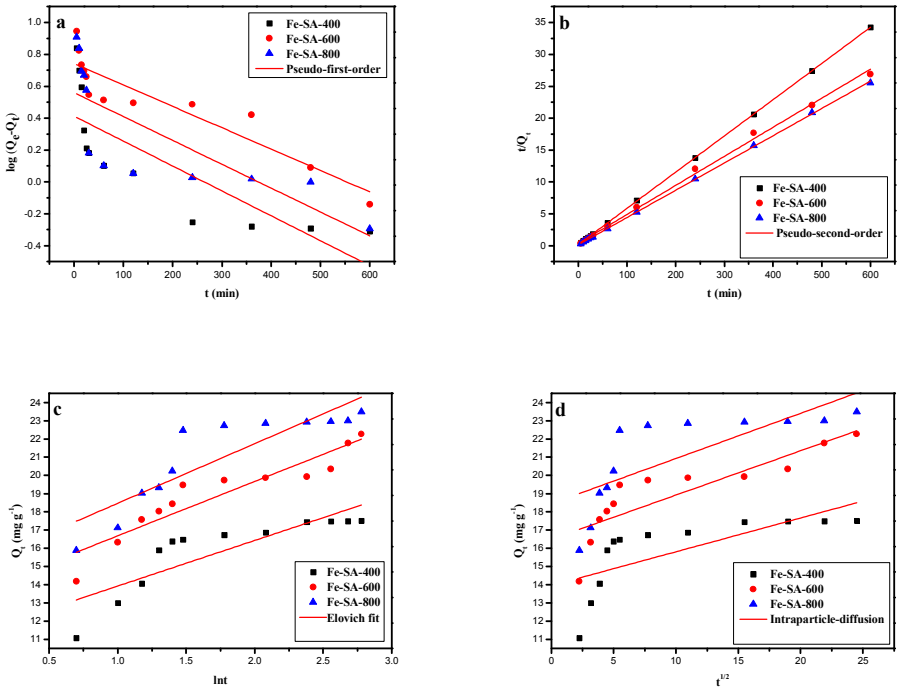

(Fig. 3.)

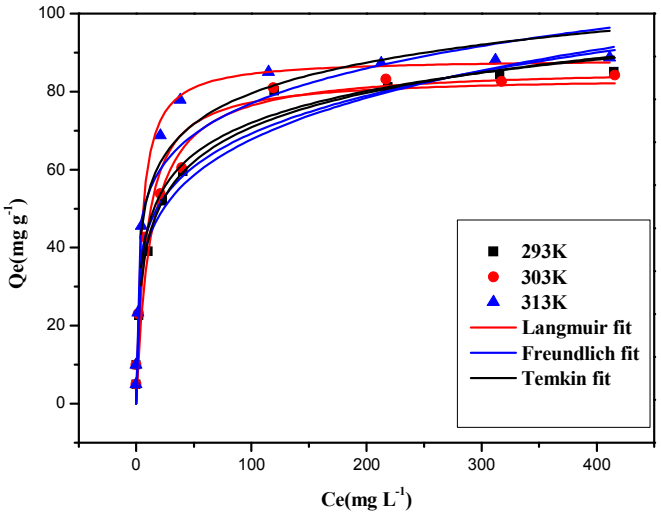

(Fig. 4.)

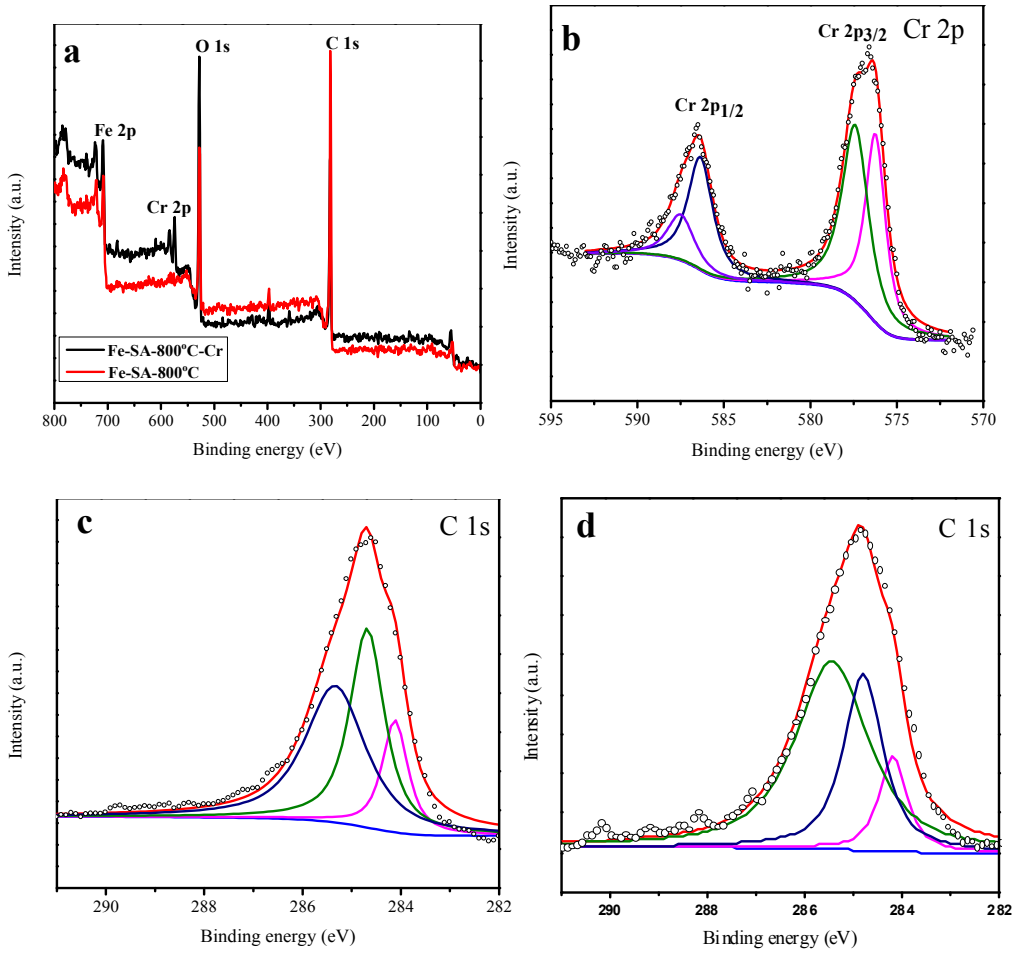

(Fig. 5.)

Table 1. The BET parameters of the Fe-SA-X.

Sample	$S_{BET}(m^2 g^{-1})$	$V_{total}(cm^{-3} g^{-1})$	$D_{peak}(Å)$
Fe-SA-200	18.206	0.076	48.9
Fe-SA-400	146.857	0.217	42.1
Fe-SA-600	183.496	0.243	37.7
Fe-SA-800	203.106	0.276	28.8

Table 2**.** Kinetic parameters of Cr(VI) adsorption on the Fe-SA-X.

Kinetics	Parameters	Fe-SA-X		
		400	600	800
Pseudo-first-order	$Q_{e,exp}(mg g^{-1})$	17.51	22.28	23.49
	$K_1(min^{-1})$	0.0036	0.0030	0.0034
	$Q_{e,cal}(mg g^{-1})$	2.58	5.53	3.63
	R^2	0.62	0.84	0.58
Pseudo-second-order	K_2 $(g mg^{-1}min^{-1})$	0.019	0.006	0.013
	$Q_{e,cal}(mg g^{-1})$	17.59	21.94	23.39
	R^2	0.99	0.99	0.99
Elovich equation	a	243.59	289.39	334.01
	b	0.39	0.34	0.31
	R^2	0.70	0.85	0.76
Intraparticle-diffusion	K_i	0.19	0.24	0.25
	C	13.9	16.5	18.5
	R^2	0.45	0.69	0.52

Table 3. Isotherm parameters of Cr(VI) adsorption on Fe-SA-800.

Isotherm models	Parameters	Temperature(K)		
		293	303	313
Langmuir	Q_m(mg g^{-1})	86.32	83.85	86.30
	K_L(L mg^{-1})	0.077	0.118	0.207
	R^2	0.971	0.974	0.965
	R_L	0.025-0.721	0.017-0.629	0.009-0.492
Freundlich	K_F(mg g^{-1})	25.69	28.97	34.20
	n	4.747	5.284	5.862
	R^2	0.955	0.951	0.936
Temkin	A(L mg^{-1})	2.57	4.72	11.15
	B(mg g^{-1})	12.77	11.70	11.34
	R^2	0.963	0.961	0.955

Table 4 The Cr(VI) adsorption capacity of Fe-SA-800 compared with other similar materials

Adsorbent	Adsorption capacity (mg g^{-1})	Reference
N-ACs	89	38
Bt/Bc/α-Fe_2O_3	81.7	39
CMB	120	40
Oxi-MWCNTS	85.83	41
Fe @ PC	10	16
RHC-mag-CN	16	42
Fe_3O_4@Alg-Ce	14.29	13
Fe_3O_4/CNT-IL	55.43	43
Fe-SA-800	86.32	This work